UCRL--95866

DE87 004357

SHOCK WAVE INTERACTION WITH TURBULENCE PSEUDOSPECTRAL SIMULATIONS*

Alfred C. Buckingham
Lawrence Livermore National Laboratory, University of California
Livermore, California 94550

ABSTRACT

Shock waves amplify pre-existing turbulence. Shock tube and shock wave boundary layer interaction experiments provide qualitative confirmation. However, shock pressure, temperature, and rapid transit complicate direct measurement. Computational simulations supplement the experimental data base and help isolate the mechanisms responsible. Simulations and experiments, particularly under reflected shock wave conditions, significantly influence material mixing. In these pseudospectral Navier-Stokes simulations the shock wave is treated as either a moving (tracked or fitted) domain boundary. The simulations assist development of code mix models. Shock Mach number and pre-existing turbulence intensity initially emerge as key parameters.

I. INTRODUCTION

Shock waves may create turbulence (at appropriate flow Reynolds numbers). Shocks may also amplify or enhance pre-existing turbulence. This phenomena is well established and recognized in shock tube and supersonic wind tunnel experiments. Shock wave enhancement of turbulent material mixing is the central issue in this work.

While the presence of shock waves and their substantial influence on the turbulent flow field has probably frustrated experimentalists for over forty years, systematic analysis appears to have awaited the study of sonic acoustical noise generation. Moore[1] and Ribner,[2] almost simultaneously, formulated the theoretical interaction of a shock wave with an inviscid (Euler's equations) compressible flow field. Ribner subsequently expanded his analysis to include spectral shock wave turbulent flow field interaction information. It was determined that imposition of any single one of three possible flow disturbances: entropy (random density fluctuations), vorticity (random velocity fluctuations), or sound-acoustics (random pressure fluctuations), give rise to all three fields after passage through a shock front. The pre-existing disturbance is substantially amplified and the wave phase is altered.

The first numerical studies included finite-difference methods applied to shock tube and blast wave reflection processes[3] and to shock-wave boundary layer interaction processes.[4] McKenzie and Westphal developed a linear theory for shock interaction with pre-existing, weakly disturbed fields using a small perturbation to the shock jump conditions.[5] These informative results apply strictly to low levels of pre-existing turbulence amplified at a plane, undeformed shock front.

Experimentally, it is evident that shock fronts deform substantially after encounters with a randomly disturbed media. The resulting non-linear interaction may lead to even greater disturbance amplitude enhancement than that predicted by the linear theory.

Other pertinent theoretical/analytical work includes application of rapid (strain) distortion theory to shock-wave turbulent boundary layer interactions.[6] The classic description focusing theoretical attention on the physics of turbulence shock boundary layer interaction was probably that provided by Kovasznay's analysis and review of physical observations nearly thirty-five years ago.[7]

Experimentally, flow visualization techniques provide considerable insight into the shock turbulence amplification processes associated with wave deformation, wave diffraction and consequent focusing of

* Work performed under the auspices of the U.S. Department of Energy by Lawrence Livermore National Laboratory under Contract #W-7405-Eng-48.

transmitted pre-existing disturbances.[8,9] Recently hot wire anemometry has been applied, using slack, relatively coarse hot wires for direct measurement of fluctuating components during shock tube shock transit.[10,11]

Measured turbulence amplification levels of the order of a 5-fold or more increase over pre-shocked values are illustrated in Fig. 1. These data include density $\langle\rho\rangle$ (entropy), velocity $\langle u\rangle$ (vorticity), and mass flux $\langle\rho u\rangle$ rms fluctuation levels. They are measured, commonly, at low Mach numbers and low pressure levels of 1 atmosphere or less. Furthermore, the instantaneous corrections for the shock pressure resistant slackened hot wire motions, the temperature jump corrections and the short duration of the test period of stationary flow at a probe site add to measurement uncertainties and limits on resolution. The Mach number and pressure range tested are well below those of common interest. The experimental limits of low Mach number and pressure, together with the low turbulence intensity* (<1%) developed in shock tube experiments are added reasons for developing reliable numerical simulations.

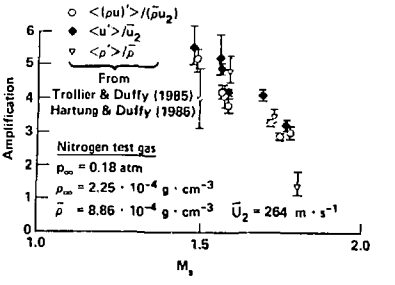

Fig. 1. Shock wave enhanced turbulence observed in shock tube experiments.

In these and subsequent figures, the shock Mach number, M_s, which is the ratio of shock speed to average "quiescent" sound speed ahead of the shock, is used as the shock strength parameter. The other significant parameter, local Reynolds number, is treated as an implicit variable associated with the flow conditions.

Aside from the pressure level, flow Mach number, and probe error uncertainties, direct shock tube measurements of turbulence are difficult to interpret properly. The basic problem is that the total interval of nearly stationary flow available at the probe site is far too short to permit resolution of more than 5% to 10% of the spectrum necessary to adequately describe the turbulence.[12]

Available experimental observations on shock turbulence interaction include a substantial number of shock turbulence boundary layer measurements. These boundary layer data on flow separation, heat transfer, and aerodynamic noise generation represent studies completed over the last thirty or more years.[7,13,14,15] Unfortunately, interpretation of these boundary layer interactions require assumptions about momentum and energy coupling and exchange mechanisms which are poorly understood at this time. Consequently they are subject to even greater error than the analysis of shock wave free shear turbulence interactions, discussed previously.[12]

Nonetheless, comparisons are provided here using theoretical assumption on boundary layer separation, surface shear, and heating to supplement the available shock tube data. In the analysis it was assumed that there existed direct and irreversible (no thermal dissipation) coupling of the rotational momentum supplied by shock wave interaction to induce the measured separation. To this extent these boundary layer interaction estimates are conservative. Larger values of shock turbulence amplification probably exist in the actual physical situation than those estimated.

II. DISCUSSION

A. The Problem

Notice that Fig. 2 shows an expanded Mach number range in comparison to that of Fig. 1, described previously. Figure 2 also contains the previously discussed boundary layer shock interaction amplification

* Turbulent intensity is defined here as the ratio of the root mean square of some fluctuating component, viz. $\langle\phi'\rangle$, to its long-time averaged mean value, $\bar{\phi}$. It is referred to here as a percentage of this mean value.

data. For qualitative guidance a plot of results of the linear theory,[5] for a $\gamma = 7/5$ ideal gas, is provided. This appears as the solid curve in the figure. The shock tube results for random velocity (vorticity) amplification are singled out for analysis here.

It can be seen that linear theory predicts peak amplification around Mach number of 6. This appears to be followed by a monotonic dropoff in amplification at higher Mach numbers. The small perturbation limit on the linear theory implies a limit on the intensity of the turbulence with which the shock interacts. The undeformed planar shock assumption neglects effects of significant shock wave distortion experimentally observed, at least for low Mach number. Amplification increase with Mach number is also implied by the boundary layer data at least over the modest range of experimental Mach numbers available.

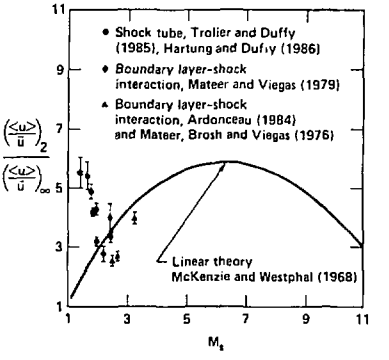

Fig. 2. Shock wave enhancement of turbulence from shock tube and wind tunnel boundary layer measurements.

The simulation requirements are, therefore, prescribed. Data is needed on the concomitant influence of increases in Mach number and initial turbulence intensity. The mode of the initial disturbance; vorticity, entropy, acoustical is presumed, for the time being to be less significant than its magnitude. However, this may be examined at a later time, once information is accumulated on the Mach number and turbulent intensity influences. The initiation of vorticity development at the shock front, the spreading of vorticity, and viscous dissipation into heat are all considered significant in the analysis. Hence, unsteady viscous (Navier-Stokes), compressible, flow simulations are developed.

B. Formulation

Neglecting body force, conservation of mass, momentum and energy for a viscous, heat-conducting, calorically perfect ideal continuum fluid are expressed in Cartesian coordinates, x^1, i=1,2,3, for unsteady non-uniform density, $\rho(x^i,t)$, and flow velocity, $u^i\ (x^i, t)$:

$$\rho_{,t} + (\rho u^j)_{,j} = 0 \ , \tag{1}$$

$$(\rho u^i)_{,t} + (\rho u^i u^j + p\delta^{ij} - \tau^{ij})_{,j} = 0 \ , \tag{2}$$

$$(\rho e)_{,t} + (\rho e u^j \delta^{ij} + p u^j \delta^{ij} - q^j \delta^{ij})_{,j} - \Phi = 0 \ , \tag{3}$$

$$\delta^{ij} = \begin{cases} 1 \ , & i=j \ , \\ 0 \ , & \text{otherwise} \ . \end{cases}$$

In the foregoing, subscripts (,t ,j) denote partial derivatives with respect to time and spatial coordinates, respectively. The pressure is denoted by p, the specific internal energy by e and the heat flux vector by,

$$q^j = k_\theta^\circ \theta_{,j} \ , \tag{4}$$

where k_θ is an associated thermal conductivity coefficient that is generally a function of temperature, θ. The stress tensor, τ^{ij}, and dissipation, Φ are defined using Stokes' hypothesis for negligible bulk viscosity*:

* The Stokes' hypothesis in which $\lambda = -\ 2/3\ \mu$ relates first and second viscosity coefficients, is adopted for simplicity at this stage. The possible influences of the neglected bulk viscosity may be examined in a later stage of our analysis.

$$\tau^{ij} = \mu^o \left[(u^i_{,j} + u^j_{,i}) - \frac{2}{3} \delta^{ij} u^i_{,j} \right] , \tag{5}$$

$$\Phi = (\tau^{ij} u^j \delta^{ij})_{,j} . \tag{6}$$

For a direct simulation of all fluctuating scales of motion on a computational grid, the molecular or shear viscosity coefficient, μ^o, may be rescaled as large as necessary to provide only viscous dissipation at the sub-grid scale level. All explicit motions are thereby resolved on the grid. In the present trials this is accomplished by limiting the flow Reynolds number to 1000. The rescaled $\mu = \mu^o \times$ (scale factor) is given by,

$$\mu = (\delta_2 \, u_2 \, \lambda)/1000 . \tag{7}$$

Here, the wavelength λ is prescribed to be the span width.

For a 10% post-shock flow disturbance (vorticity) intensity, we may estimate the turbulence Reynolds number at this scaled viscosity level, and from that the minimum number of modes necessary to resolve all scales on the resulting grid. This number is 14. To be conservative and alias-free we prescribe 32 modes in each space dimension. Consistent viscous dissipation requires that the turbulent eddy conductivity must be proportionately rescaled. This is accomplished by specifying a unit turbulent Prandtl number, hence,

$$k_\theta = k^o_\theta \cdot \text{scale factor} = \mu\gamma \frac{e}{\theta} . \tag{8}$$

Here we have assumed a calorically perfect ideal gas with polytropic exponent, $\gamma = 7/5$.

Two pseudospectral methods are used. The earliest coded method, a "shock-capturing" procedure is less accurate than the second, a "shock-fitting" procedure, but is much easier to implement. It provides the present trial simulation results. The second method is under current development. Both will be outlined. Use of pseudospectral methods for shock-turbulence interaction studies is in part stimulated by the recent inviscid (Euler equation) developments of Zang et al.[16,17] Our work extends this to study of viscous (Navier-Stokes) flow.

In both the shock capturing and shock fitting procedures, the viscous conservation equations, Eqs. (1)-(3), are expanded in a two-dimensional Cartesian, x,y (streamwise, spanwise) plane. For computational convenience, the following dimensionless variables are introduced:

$$\rho = \rho^o/\bar{\rho}_2, \; u,v = u^o, v^o/\bar{u}_2, \; e = e^o/(\bar{u}_2)^2, \; p,\tau = (p^o,\tau^o)/(\bar{\rho}_2\bar{u}_2^2), \; q = q^o/(\bar{\rho}_2\bar{u}_2^3) , \tag{9}$$

while $x,y = (x^o,y^o)\times(2\pi/\lambda)$.

In the foregoing, superscript zeroes designate dimensional variables, while barred variables with subscript "2" refer to mean values behind the advancing shock, S, shown as a vertical line in Fig. 3. The wavelength, λ, is the spanwise dimension of the computational grid, with periodic boundary conditions applied at extremum. Inflow boundary conditions supporting an advancing plane shock at prescribed Mach number are applied at $x = 0$. Impermeable wall boundary conditions are applied at the right-hand boundary ($x = \underline{X}$ with reference to Fig. 3).

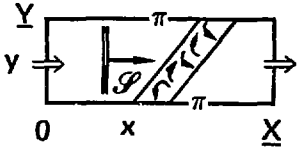

Fig. 3. Sketch of flow and computational configuration for Method 1.

In the Cartesian plane the conservation equations (1), (2), and (3) are expanded in the form of vectors: A, B, C, D:

$$A_{,t} = B_{,x} + C_{,y} + D , \tag{10}$$

whose components are the respective derivative terms produced from expanding Eqs. (1) through (3). Considering space limitations, discussion is restricted to outlining the procedure through use of the

symbolic vector operator form given by Eq. (10). For more algebraic detail, a somewhat parallel vector formulation is provided in Ref. 18 for pseudospectral Euler equation simulations on Kelvin-Helmholtz and Rayleigh-Taylor instabilities.[18] Specialized treatment of the viscous stress terms and the operational algebra will appear in subsequent publications.

In Method 1, the "shock capturing" procedure, artificial viscosity, q, and necessary, albeit, limited, selective high wave number filtering add sufficient viscous damping for stability. These factors compensate for the neglected von Neumann-Richtmyer artificial viscosity.

At each discrete time interval NΔt, for $t \geq 0$, the shock wave bounded spatially continuous functions: u, ρ, e, etc. are represented streamwise by truncated Chebyshev series and spanwise by truncated Fourier series. Dependent variables and their derivatives are given by their spectral representations with respect to these basis functions following FFT projection into the phase plane. Symbolically, the compound two dimensional basis function operations are given by the series truncated at P,M = 32 in our tests:

$$\phi^N(x, y, t) = \sum_{p=0}^{P} \sum_{m=0}^{M} \phi^N(p, m, t)\, T_p(y) \exp\{2\pi i m \tfrac{x}{\bar{x}}\} \qquad (11)$$

Here the Chebyshev function is represented by, $T_p(y) \equiv \cos(p \cos^{-1} y)$.

Inverse FFT transformation to the physical plane precedes evaluation of the non-linear products: $u \cdot u$, $u \cdot v$, $u \cdot u_x$, etc. The spatially dependent terms, derivatives and products form the right hand side of the symbolic operational tendency equations (10). Subsequently the tendency equation is updated from NΔt to (N + 1)Δt, explicitly in time, using a third order Runge-Kutta procedure.

Convergence of the procedure requires operations approaching N ln N for the Nth truncation rather than p^N required for the most rapid polynomial discretization operations.

The first procedure outlined introduces errors from the ill-posed shock-discontinuity which grossly violates the continuous and smooth characteristic functional behavior strictly required for spectral methods. Global oscillations develop from the localized discontinuous interruption of functional smoothness at shock fronts and boundaries. Gibb's phenomena and, perhaps, to a lesser extent, numerically diffusive spreading of the shock wave over two or more grid points in the shock capturing procedure contaminate the numerical results.

To limit this error contamination and recover the resolution potentially available for continuous and smooth (uninterrupted) functional behavior of all dependent variables, the discontinuous shock wave front, S, should be treated as a moving outer boundary to the computational domain. The second method, suggested by the moving shock/boundary coordinate system developed by Zang et al.,[16,17] appears to resolve this difficulty, although at the cost of a considerable increase in the computational and formulation effort.

In Method 2 (with reference to Fig. 4) the computational domain in x,y space is split into two regions. Region 2 is downstream of a moving shock front, S, and Region 1 is upstream. The initial vortical disturbance is applied ahead of the advancing shock front, as depicted, similar to Method 1. However, the discontinuous shock boundary is now a moving outer boundary to Region 1. The Rankine-Hugoniot jump conditions instantaneously prescribe the motion and deformation of this boundary and simultaneously establish boundary conditions on the interior solution of the shocked domain (Region 1). The ill-posedness is offset by requiring, at each discrete time interval, a method-of-characteristics[19] compatibility between the to-be-determined shock front position, the jump conditions, the downstream conditions and the upstream (subsonic, hence influentially elliptic) conditions. The shock profile and position is determined in x, y, and t

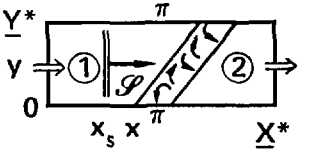

Fig. 4. Sketch of flow and computational configuration for shock-fitting Method 2.

compatible with these conditions through a method-of-characteristics shock-fitting procedure adapted from stationary shock solutions[20] but modified by use of the appropriate acceleration as opposed to stationary shock front conditions.[16,17]

A key step in Method 2 which provides for shock deformation from non-uniform flow is the mapping from the fixed Cartesian x,y coordinate system to a moving coordinate system, $\hat{x}$, $\hat{y}$. The mapping involves tracking and fitting the shock front profile x_s (y, t).

The remapped configuration space with the shock as an outer boundary is defined by

$$\hat{X} = x - x_o\ (t)/(x_s\ (y,\ t) - x_o\ (t)) \quad \text{and} \quad \hat{Y} = y/Y^* \ , \tag{12}$$

as indicated in Fig. 4, while the corresponding contravariant velocity components are computed from,

$$\hat{u}^i = \hat{X}_{,t} + u^i\ \hat{X}_{,x} + u^j \hat{X}_{,y} \ ; \ \hat{u}^j = \hat{Y}_{,t} + u^i\ \hat{Y}_{,x} + u^j\ \hat{Y}_{,y} \tag{13}$$

C. Results

Method 1 provides "inviscid" results by use of an artificial viscosity, "Q" (and corresponding neglect of physical viscosity, $\mu = 0$). Q is quadratically proportional to the grid mesh collocation streamwise spacing at the shock front in parallel with the pro edure used for the hybrid Euler-Lagrange pseudospectral instability results.[18] These results are plotted as the filled diamond symbols for various Mach numbers in Fig. 5. They are compared with the Zang et al.[16,17] results for inviscid shock-fitting and the linearized theoretical results of McKenzie and Westphal[5] which Zang et al. match closely. The experimental data are enveloped by the cross hatched region on the plot. Significantly more amplification of the initial disturbance at low Mach number and more dissipation at higher Mach number are predicted from our present "inviscid" but artifically spread, "Q"-damped, shock-capturing results. These results are, of course, somewhat suspect because of the numerical contamination associated with shock capturing, discussed previously.

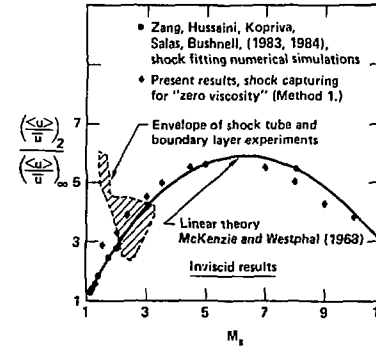

Fig. 5. Shock wave enhancement of turbulence. Comparison of simulations, experiment and linear theory in inviscid flow.

Figures 6 and 7 show the absolute (rms) values of vorticity at specified positions behind the shock front in comparison to the initial disturbance level (indicated by the arrow designation at the shock

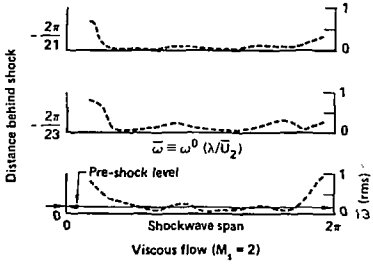

Fig. 6. Simulations of vorticity amplification by a Mach 2 shock wave at several positions behind shock in viscous flow.

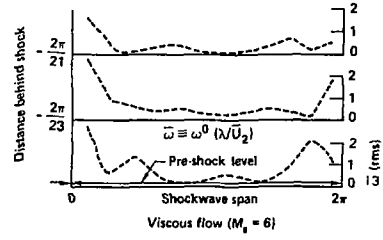

Fig. 7. Simulations of vorticity amplification by a Mach 6 shock wave at several positions behind shock in viscous flow.

front. These results are for Mach Nos. 2 and 6, respectively. This initial level is the perturbation value applied in the quiescent free stream ahead of the shock. These viscous flow results are developed over a period of time sufficiently long so as to entrain and amplify the entirety of the ambient upstream initial disturbance.

In a summary plot, Fig. 8, we show the results of the viscous flow simulations at several Mach numbers within the Mach number range from $M_s = 2$ to 10. The inviscid Method 1 results (diamonds) are plotted in comparison to the viscous Method 1 results (triangles). The linear theory is shown as a solid curve.

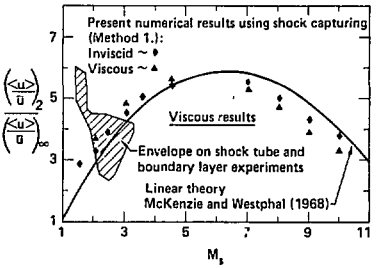

Fig. 8. Shock wave enhancement of turbulence. Comparison of simulations, experiment and linear theory in viscous flow.

Generally, the viscous results appear to predict more shock deformation at low Mach number and more dissipation, with relatively decreased amplification at higher mach number in comparison to the inviscid results for Method 1.

It is the intent here to further examine this shock interaction as a function of initial disturbance intensity and Mach number effect. The current analysis will make use of the potentially more accurate viscous, shock-fitting results of Method 2. Subsequently, substantially higher resolution, hence higher Reynolds number flows may be simulated by use of increased modal resolution. In this regard, about a 256x256 resolution in modal expansion appears to be necessary to provide results equivalent for flow Reynolds numbers slightly greater than 12000 in future computations.

D. Summary

In our, admittedly, preliminary results we have learned several useful pieces of information pertaining to shock amplification of initial flow disturbances. We submit the following:

- Intensely disturbed initial flows distort low Mach number shock waves severely. They consequently generate substantial amplification of the disturbance and intensify mixing behind to shock. Shock front break-up, and resulting diffraction and focusing of incident disturbances appear significant.
- The dissipation of the turbulent kinetic energy, however, is also substantially enhanced by transition through a shock wave. Hence the duration of the shock-enhanced turbulent kinetic energy may be reduced, particularly as shock strength increases.
- The captured finite shock front locally contaminates numerical results with low-order errors when using spectral projection or any discrete numerical method with an artificial viscosity.
- Spectral projection methods amplify these local shock front errors globally.
- A shock-fitting procedure, treating the shock front as a real boundary to the computational domain, appears to be the appropriate method for alleviating these spread shock wave induced errors.

ACKNOWLEDGMENTS

The writer gratefully acknowledges the guidance, criticism, challenges and support provided by J. Bolstad, E. W. Burke, W. P. Crowley, C. E. Leith, L. Margolin, V. Rupert, P. Stry, and the "Thursday Morning Mix Working Group". Particular thanks are given to Margaret Dixon who prepared, edited, and provided the publication lay-out for this manuscript with her characteristic accuracy and dispatch.

REFERENCES

1. Moore, F. K. (1954) "Unsteady Oblique Interaction of a Shock Wave with a Plane Disturbance," National Advisory Committee for Aeronautics Rept. NACA-TR-1165.
2. Ribner, H. S. (1955) "Shock Turbulence Interaction and the Generation of Noise," National Advisory Committee for Aeronautics Rept. NACA-TR-1233.
3. Scala, S. M. and Gordon, P., (1966) "Reflection of a Shock Wave at a Surface", Phys. of Fluids 9 (6), 1158-1166.
4. Baldwin, B. S. and MacCormack, R. W. (1974) "Numerical Solution of the Interaction of a Strong Shock Wave with a Hypersonic Turbulent Boundary Layer," AIAA Paper No. 74-558 (Archival) in AIAA 7th Fluid and Plasma Dynamics Conf., Palo Alto, CA.
5. McKenzie, J. F. and Westphal, K. O. (1968) "Interaction of Linear Waves with Oblique Shock Waves," Phys. of Fluids 11, (11), 2350-2362.
6. Jayaram, M., Dussauge, J.-P., and Smits, A. J. (1985) "Analysis of a Rapidly Distorted, Supersonic, Turbulent Boundary Layer," in Fifth Symposium on Turbulent Shear Flows, Cornell Univ., Ithaca, NY, 1-8.
7. Kovasznay, L. S. G. (1953) "Turbulence in Supersonic Flows," Journ. of Aerospace Sci. 20 (10), 657-674.
8. Sturtevant, B. (1977) "Shock Waves in Nonuniform Media: Real-Life Gasdynamics," in Shock Tube and Shock Wave Research, Ahlborn, Herlzberg, Russell, eds. 12-23.
9. Hesselink, L. (1977) "An Experimental Investigation of the Propagation of Weak Shock Waves Through a Random Medium, in Shock Tube and Shock Wave Research, Ahlborn, Hertzberg, Russell, eds. 82-90.
10. Trollier, J. W. and Duffy, R. E. (1985) "Turbulence Measurements in Shock-Induced Flows, AIAA Journ. 23 (8), 1172-1178.
11. Hartung, L. C. and Duffy, R. E. (1986) "Effects of Pressure on Turbulence in Shock Induced Flows," AIAA Paper No. 86-0127 (Archival) in AIAA 24th Aerospace Sciences Mtg., Reno, NV.
12. Ellzey, J. and Buckingham, A. C. (1986) "Analysis of Diagnostic Procedures for Direct Measurement of Shock Turbulence Interactions," Lawrence Livermore National Laboratory UCID (in preparation).
13. Mateer, G. G. and Viegas, J. R. (1979) "Effect of Mach and Reynolds Numbers on a Normal Shock-Wave/Turbulent Boundary-Layer Interaction," AIAA Paper 79-1502 (Archival) in AIAA 12th Fluid and Plasma Dynamics Conf., Williamsburg, VA.
14. Ardonceau, P. L. (1984) "The Structure of Turbulence in a Supersonic Shock-Wave/Boundary Layer Interaction," AIAA Journ. 22 (9) 1254-1262.
15. Anyiwo, J. C. and Bushnell, D. M. (1982) "Turbulence Amplification in Shock-Wave Boundary-Layer Interaction," AIAA Journ. 20 (7), 893-899.
16. Zang, T. A., Kopriva, D. A., and Hussaini, M. Y. (1983) "Pseudospectral Calculation of Shock Turbulence Interactions," in Proc. 3rd International Conf. on Numerical Methods in Laminar and Turbulent Flow, ed. C. Taylor, Pineridge Press, Swansea, U.K. 210-220.
17. Zang, T. A., Hussaini, M. Y., and Bushnell, D. M. (1984) "Numerical Computations of Turbulence Amplification in Shock-Wave Interactions," AIAA Journ. 22 (1), 13-21.
18. Buckingham, A. C. (1985) "Compressible Two-Phase Flow Instabilities Simulated with a Hybrid Lagrange-Euler Pseudospectral Method," in Proc 4th International Conf. on Laminar and Turbulent Flow, ed. C. E. Taylor, Pineridge Press, Swansea, U.K.
19. Ferri, A. (1949) Elements of Aerodynamics of Supersonic Flows, Macmillan Co., N.Y. Chap. 13, 261-291.
20. Buckingham, A. C. (1960) "A Real Gas Method of Characteristics Program," Douglas Aircraft Co. Re-entry Gas Dynamics Research Report SM-38078, Santa Monica, CA.